Proteomic Profiling of Fibroblasts Isolated from Chronic Wounds Identifies Disease-Relevant Signaling Pathways

JID Open

Bettina Berberich[1,4], Kerstin Thriene[1,2,4], Christine Gretzmeier[1], Tobias Kühl[1], Hans Bayer[1], Ioannis Athanasiou[1], David Ali Rafei-Shamsabadi[1], Leena Bruckner-Tuderman[1], Alexander Nyström[1,5], Dimitra Kiritsi[1,5] and Jörn Dengjel[1,3,5]

Chronic skin wounds accompany many prevalent age-related diseases and are a major cause of morbidity and mortality. Both keratinocytes and fibroblasts contribute to the pathomechanisms in chronic skin wounds. Dysregulated pathways in the epidermis have been extensively studied, but little is known of the influence of dermal fibroblasts on chronic wounding. We isolated fibroblasts from chronic wounds, propagated them in vitro, and analyzed them using proteomic profiling in combination with functional characterization of the proteomic changes. Chronic wound–associated fibroblasts exhibit a unique proteome profile characteristic of lysosomal dysfunction and dysregulated TGFβ signaling. They display a decreased propensity for cell proliferation and migration, combined with an enhanced ability to contract the extracellular matrix. With these properties, chronic wound–associated fibroblasts actively contribute to pathological inabilities to close wounds and represent potential targets for pharmacological interference for changing cellular phenotypes.

Journal of Investigative Dermatology (2020) **140,** 2280–2290; doi:10.1016/j.jid.2020.02.040

INTRODUCTION

Physiological skin wound healing is a complex process requiring coordination and regulation both in time and in space between the participating cell types and their expressomes. Deviation from the strict regulation leads to faulty healing, which represents a major and growing cause of morbidity and mortality. In Western societies, the increasing age of populations and incidence of lifestyle diseases, such as diabetes and obesity, are associated with defects in wound repair and will further increase incidence rates.

Immediately after skin wounding, homeostasis is initiated to preserve organ function and to protect the affected individual from fluid loss and invading pathogens. Wound healing is traditionally divided into three main phases: (i) in the inflammation phase, a first wave of neutrophils and subsequently macrophages are recruited. These cells defend the damaged tissue against invading pathogens but also release growth factors and cytokines. These promote (ii) the tissue-regenerating proliferative phase of wound healing. During this phase, keratinocytes are the first skin-specific cells that become activated. They migrate beneath the fibrin clot to close the epidermal gap. Finally, (iii) remodeling and differentiation of the new skin occurs (Shaw and Martin, 2016).

Dermal healing lags behind epidermal healing, and proliferation of dermal fibroblasts and migration into the wound is initiated after re-epithelialization is well on its way (Gurtner et al., 2008). During dermal wound healing, a loose and highly vascularized granulation tissue fills the dermal part of the wound; the increased vascularization reflects the elevated metabolic need of the regenerating tissue (Shaw and Martin, 2016). This tissue is subsequently strengthened by deposition of a rather disorganized provisional extracellular matrix (ECM) by wound-associated fibroblasts (Chester and Brown, 2017; Shaw and Martin, 2016), which are the first major mesenchymal-derived cells to populate the regenerating dermis. For wound contraction and closure, myofibroblasts, which are derived from fibroblasts after TGFβ exposure and which express smooth muscle actin, are of vital importance (Desmoulière et al., 1993; Pakshir and Hinz, 2018). Myofibroblasts contract the wound and increase ECM density, thus promoting tissue strength (Eming et al., 2014; Pakshir and Hinz, 2018). The inability to properly execute the proliferative phase to enable wound closure leads to formation of chronic wounds. These are defined as persisting for minimally three months, in contrast to acute wounds, which heal commonly within three weeks (Pang et al., 2017).

So far, treatment of wound healing disorders is largely limited to symptomatic and not pathogenesis-based therapies, mainly because the molecular and cellular processes underlying wound repair are still insufficiently understood

[1]Department of Dermatology, Faculty of Medicine, Medical Center - University of Freiburg, Freiburg im Breisgau, Germany; [2]Institute for Prevention and Cancer Epidemiology, Faculty of Medicine, Medical Center - University of Freiburg, Freiburg im Breisgau, Germany; and [3]Department of Biology, University of Fribourg, Fribourg, Switzerland

[4]These authors contributed equally to this work.

[5]These authors contributed equally to this work.

Correspondence: Jörn Dengjel, Department of Biology, University of Fribourg, Chemin du Musée 10, 1700 Fribourg, Switzerland. E-mail: joern.dengjel@unifr.ch

Abbreviations: 5-aza, 5-azacytidine; aWAF, acute wound–associated fibroblast; cWAF, chronic wound–associated fibroblast; ECM, extracellular matrix; MS, mass spectrometry; NHF, normal human fibroblast; ruxo, ruxolitinib

Received 8 November 2019; revised 10 February 2020; accepted 26 February 2020; accepted manuscript published online 17 April 2020; corrected proof published online 29 May 2020

(Schäfer and Werner, 2008). Most causal therapy efforts thus far have focused on achieving re-epithelialization by stimulation of keratinocytes with growth factors or application of wound dressings and biomaterials that promote keratinocyte migration (Widgerow, 2013). However, because most of the skin's unique strength and elastic properties are attributed to the dermis (Has and Nyström, 2015), such therapies will only have long-lasting beneficial effects when dermal healing is also adequately restored. Currently, this remains a challenge. The basic dynamics of dermal healing were previously thought to be relatively simple, with fibroblasts at the wound edge becoming activated to repopulate the injured dermis by proliferation and migration and to restore the dermal matrix by synthesis and deposition of ECM proteins (Shaw and Martin, 2016). It is now emerging that this process is more complex than formerly anticipated, involving different fibroblast lineages (Driskell et al., 2013).

Here, we took a proteomics approach to define chronic wound–associated fibroblasts (cWAFs) and analyzed fibroblasts from chronic wounds vis-à-vis control fibroblasts, acute wound–associated fibroblasts (aWAFs), and myofibroblasts. cWAFs were severely damaged and clearly different from normal skin–resident fibroblasts, as shown by their unique proteome profile. Our study provides support that chronic wounds—at least a subset of them—evolve as a partially fibroblast-driven disease. We propose that the distinct cellular phenotype of cWAFs is generated from resident fibroblasts responding to chronic damage and inflammation, and that these cells actively contribute to pathogenesis of chronic wounds in a manner that is conceptually similar to cancer-associated fibroblasts in cancer progression.

RESULTS

Proteomic profiling reveals dysregulated processes in cWAFs

We have shown previously that human dermal fibroblasts remain phenotypically stable in culture for several weeks and thus are amenable for proteomic analyses using metabolic labeling strategies (Küttner et al., 2013; Sprenger et al., 2010). For this study, we used primary dermal fibroblasts from the wound edge of chronic leg ulcers from five donors, referred to as cWAFs, and fibroblasts from six control donors, here referred to as normal human fibroblasts (NHFs). Female and male donors were used for both cellular phenotypes. cWAF donors were between 39 and 91 years old, and cells were derived from the lower leg. The NHF donors were 50 to 81 years old at the time of the biopsies (Table 1).

To test if cWAFs exhibit a unique molecular signature that is maintained after isolation of cells from punch biopsies and that helps understanding the processes underlying the failure of cWAFs to support dermal healing, we performed global expression proteomics analyses using a standard bottom-up proteomics workflow (Figure 1a). NHFs and cWAFs were metabolically labeled by stable isotope labeling by amino acids in cell culture, and in combination with a light-labeled SUPER–stable isotope labeling by amino acids in cell culture spike-in mix, all samples were compared with each other (Figure 1a) (Geiger et al., 2010). Each cell type was analyzed twice with swapped labels to exclude labeling artifacts (Supplementary Figure S1). In total, we identified 3,446 protein groups, of which 984 were present in all samples (Supplementary Table S1). A principle component analysis of the individual samples revealed that NHFs and cWAFs separated into two distinct groups (Figure 1b). This was also the case for a hierarchical cluster analysis of protein abundances, which resulted in five clusters in which abundances were distinct between the two cellular phenotypes (Figure 1c). Analysis of Gene Ontology terms covering biological processes and cellular components revealed processes potentially being involved in the failure of cWAFs to promote proper dermal healing. Thus, proteins involved in cell adhesion, ECM organization, and lysosomal components were highly increased in cWAFs compared with NHFs (clusters 4 and 5, Figure 1c). In contrast, proteins involved in gene expression, RNA processing, and translation appeared depleted in cWAFs, indicating a general decrease in metabolic activity (clusters 2 and 3, Figure 1c; Supplementary Tables S2–S5).

Table 1. Characteristics of Primary NHFs, cWAFs, and aWAFs Used in This Study

Cell ID	Age at Biopsy	Sex	Biopsy Location	Diagnosis
NHF1	50	Male	groin	healthy
NHF2	63	Female	groin	healthy
NHF3	86	Female	thigh	healthy
NHF4	74	Female	thigh	healthy
NHF5	61	Male	shoulder	healthy
NHF6	81	Female	forearm	healthy
cWAF1	75	Female	leg	trauma
cWAF2	91	Female	leg	v. insufficiency
cWAF3	69	Female	leg	trauma
cWAF4	70	Male	leg	v. insufficiency
cWAF5	39	Female	leg	v. insufficiency
aWAF1	44	Female	chest	plastic surgery
aWAF2	59	Male	leg	plastic surgery

Abbreviations: aWAF, acute wound–associated fibroblast; cWAF, chronic wound–associated fibroblast; NHF, normal human fibroblast.

Focusing on proteins that were significantly upregulated in cWAFs compared with NHFs, we were able to generate a protein interaction network of 64 proteins (Figure 1d, Table 2). Proteins carrying the Gene Ontology term "wound healing" were significantly enriched in this network, highlighting the source of analyzed cells (false discovery rate $<$ 0.001). In agreement with the cluster analysis, proteins involved in cell adhesion, such as several integrins, were significantly more abundant in cWAFs than NHFs.

We also compared the proteomic composition of cWAFs to NHFs treated with TGFβ as a model for myofibroblasts as well as to aWAFs, and analyzed the expression of fibroblast lineage marker proteins defined in mouse models (Driskell et al., 2013). cWAFs exhibited a distinct cellular phenotype that was maintained in vitro and differed from myofibroblasts and aWAFs (Supplementary Figure S2). Also, their membrane proteome could not be linked to a specific fibroblast lineage or subpopulation (Driskell et al., 2013; Tabib et al., 2018). cWAFs expressed both reticular and papillary fibroblast markers, such as TGM2 and DPP4/CD26, respectively (Supplementary Figure S2). Thus, it appears that cWAFs

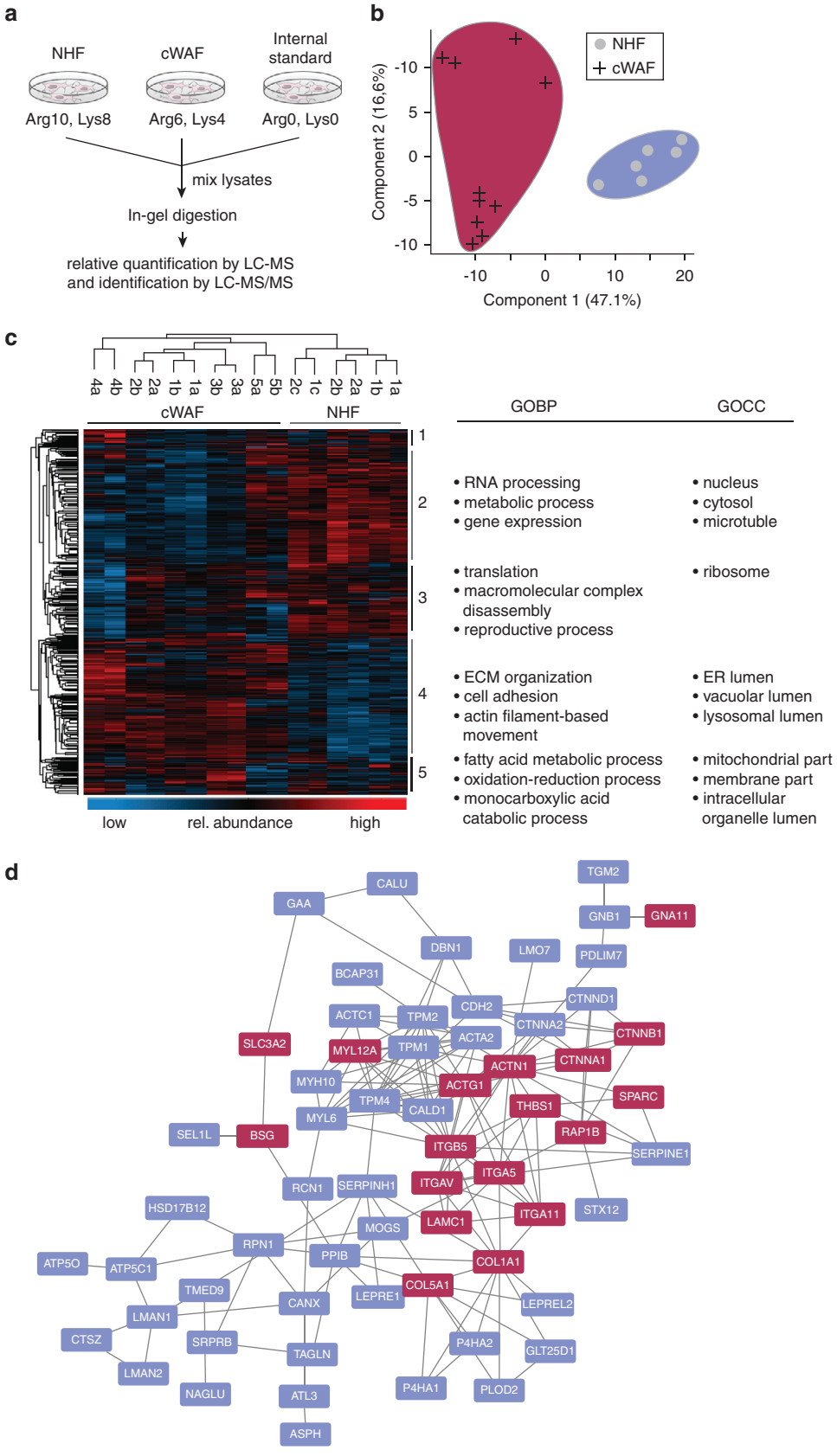

Figure 1. Expression proteomics analysis comparing cWAFs and NHFs reveals cell phenotype-specific proteomic signatures. (**a**) SILAC-based quantitative MS workflow. All cell cultures were combined to a Super-SILAC mix (light; heavy) as a reference. This internal standard was spiked in 1:1:1 ratio to differentially SILAC-labeled fibroblasts. The samples were processed, and peptide mixtures were analyzed using LC-MS/MS. The figure was designed using Servier Medical Art. (**b**) PCA. Log_2-transformed SILAC ratios of proteins were used. The two experimental groups are clearly separated; cWAFs show a higher diversity in component 2. (**c**) Hierarchical clustering clearly separates NHFs from cWAFs. Protein ratios were log_2 transformed and z-score normalized. Columns and rows were hierarchically clustered. Proteins in the annotated clusters were tested for enrichment of GOCC and GOBP terms and selected terms, reflecting processes related to cWAF phenotypes, are shown (full list in Supplementary Tables S2–S5. (**d**) Network analysis of significantly enriched proteins in cWAFs. Protein-protein interactions of 64 significantly enriched proteins in cWAFs as analyzed by STRING DB ($P < 0.01$; BH corrected, two-tailed, Welch-Test). Red labeled proteins carry terms "wound healing" (GOBP) and/or focal adhesion (KEGG). BH, Benjamini-Hochberg; cWAF, chronic wound –associated fibroblast; GO, Gene Ontology; GOBP, Gene Ontology biological processes; GOCC, Gene Ontology cellular components; KEGG, Kyoto Encyclopedia of Genes and Genomes; LC, liquid chromatography; MS, mass spectrometry; NHF, normal human fibroblast; PCA, principal component analysis; SILAC, stable isotope labeling by amino acids in cell culture.

Table 2. Shortlist of the Ten Most Up- and Downregulated Proteins in cWAFs Compared with NHFs

Gene Name	Protein ID	Protein Name	*P*-value	Difference [log_2 (cWAF − NHF)]
IGFBP7	Q16270	Insulin-like growth factor-binding protein 7	2.71E−07	3.63
TGM2	P21980	Protein-glutamine gamma-glutamyltransferase 2	4.64E−08	3.47
TPM1	Q6ZN40	Tropomyosin 1 (Alpha)	1.01E−08	2.97
PLOD2	O00469	Procollagen-lysine,2-oxoglutarate 5-dioxygenase 2	1.26E−04	2.72
FHOD1	Q9Y613	FH1/FH2 domain-containing protein 1	1.21E−04	2.59
TPM2	P07951-2	Tropomyosin beta chain	4.68E−08	2.41
ACTBL2	Q562R1	Beta-actin-like protein 2	1.35E−05	2.33
GAA	P10253	Lysosomal alpha-glucosidase	7.64E−07	2.27
THBS1	P07996	Thrombospondin-1	2.77E−08	2.23
CALD1	Q05682-4	Caldesmon	1.60E−07	2.21
CSPG4	Q6UVK1	Chondroitin sulfate proteoglycan 4	4.35E−03	−1.43
IPO4	Q8TEX9	Importin-4	2.61E−05	−1.44
HMGB2	P26583	High mobility group protein B2	4.54E−03	−1.45
RANBP1	P43487	Ran-specific GTPase-activating protein	3.02E−06	−1.48
EIF4H	Q15056	Eukaryotic translation initiation factor 4H	1.25E−02	−1.48
MTHFD1	P11586	C-1-tetrahydrofolate synthase, cytoplasmic	6.84E−07	−1.60
AHNAK2	Q8IVF2	Protein AHNAK2	2.66E−05	−1.67
CD109	Q6YHK3	CD109 antigen	1.64E−07	−1.73
FASN	P49327	Fatty acid synthase	1.40E−08	−2.02
FDPS	P14324	Farnesyl pyrophosphate synthase	6.59E−08	−2.15

Abbreviations: cWAF, chronic wound–associated fibroblast; NHF, normal human fibroblast.
Upregulated proteins are highlighted by gray shading.

represent a specific fibroblast phenotype exhibiting a unique proteomic signature, which is maintained in vitro and distinguishes them from other fibroblasts.

cWAFs have dysfunctional lysosomes

Lysosomal proteins appeared to accumulate in cWAFs as highlighted by the cluster analysis (Figure 1c). Specifically, the lysosome-associated glycoproteins LAMP1 and LAMP2 were significantly more abundant in cWAFs (Figure 2a). Immunofluorescence analysis of LAMP1 in cultured cells revealed that not only abundance but also distribution of LAMP1-associated lysosomes was altered in cWAFs compared with NHFs. In NHFs, LAMP1-positive lysosomes were mainly located around the cell nucleus. Contrastingly, in cWAFs, the lysosomes appeared larger and dispersed throughout the cytoplasm (Figure 2b). The altered lysosomal compartment in cWAFs could indicate two opposing functional phenotypes, (i) an increased number of active lysosomes resulting in enhanced lysosomal activity or (ii) a compensatory increase of lysosomes owing to diminished lysosomal activity. To discriminate both scenarios, we analyzed the autophagic capacity of NHFs and cWAFs under basal and starvation conditions. Abundance of the lipidated version of the autophagosome marker MAP1LC3B (LC3-II) was analyzed in the presence and absence of concanamycin A, an inhibitor of V-ATPase blocking lysosomal activity (Figure 2c). Although both cellular phenotypes responded to concanamycin A, cWAFs responded considerably weaker under basal conditions, indicating a partial block of basic autophagy and reflecting decreased lysosomal activity. In contrast, stress-induced autophagy appeared not to be affected. Thus, cWAFs exhibit an enlarged, dysfunctional lysosomal compartment reminiscent of senescent (Dörr et al., 2013) and aged cells (Dumit et al., 2014; Kilpatrick et al., 2016), which is further supported by increased abundance of beta-galactosidase GLB1 (Figure 2a), a common marker of senescent fibroblasts (Lee et al., 2006).

cWAFs exhibit an enhanced contractile ability

In culture, cWAFs displayed an enlarged cell body with multiple protrusions in contrast to the compact spindle-shaped morphology of NHFs (Figure 3a–c). They also exhibited significantly increased levels of smooth muscle actin (ACTA2), which is a common marker of myofibroblasts (Desmoulière et al., 1993) (Figure 3d). In regular wound healing, myofibroblasts are critical for wound contraction, which is profoundly reduced or absent in chronic wounds (Pang et al., 2017). As immunofluorescence analysis affirmed, increased ACTA2 levels in cWAFs (Figure 3e and f), we tested the ability of cWAFs to deform fibronectin-coated deformable silicone substrates of defined stiffness (5 kPa). In agreement with the molecular data, cWAFs were able to contract substrates in contrast to NHFs, which were unable to do so (Figure 3g).

Dysregulated TGFβ activity is a common theme in wound healing pathologies (Kiritsi and Nyström, 2018). Myofibroblasts are naturally dependent on TGFβ activity for their transformation and subsequent ability to contract ECM. However, there are also indications that TGFβ is involved in the formation of chronic wounds (Cha et al., 2008; Nagaraja et al., 2014). Analysis of phosphorylation of the canonical TGFβ signal transducers SMAD2/3 showed that TGFβ activity was indeed elevated in cWAFs (Figure 3i), in agreement with the observed cellular phenotype. To further investigate what could contribute to the increased TGFβ signaling in cWAFs, we screened the proteomics data for proteins known to be involved in regulation of its activity. The cell surface receptor CD109, which downregulates TGFβ activity by internalizing the TGFβ receptors 1 and 2 (Bizet et al., 2011), was reduced in cWAFs (Supplementary Figure S2). TGFβ is secreted as a latent molecule that needs to undergo enzymatic or mechanic activation (Hinz, 2015). Thrombospondin-1, a latent TGFβ activator (Murphy-Ullrich and Downs, 2015) that has been shown to be upregulated in chronic ulcers versus healing ulcers (Charles et al., 2008), was increased in cWAFs (Supplementary Figure S2). Collectively, the data indicate that the increased TGFβ activity in cWAFs is

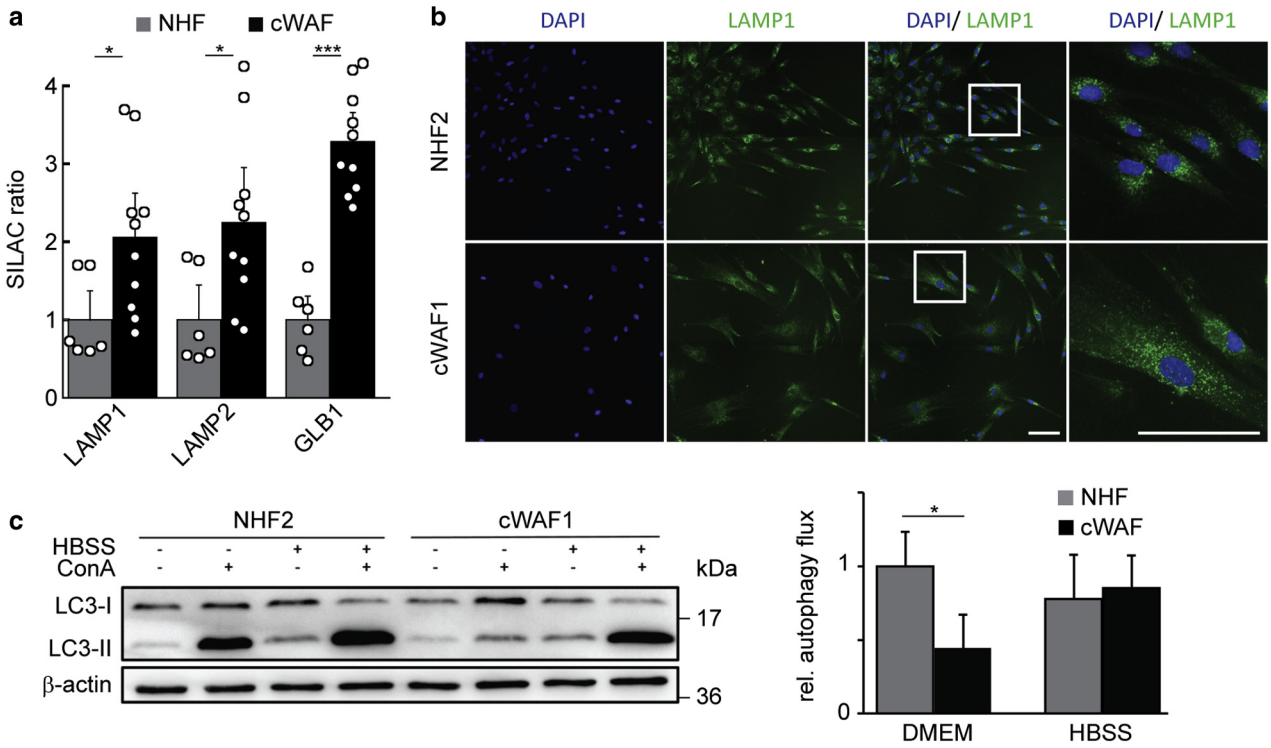

Figure 2. cWAFs exhibit an altered lysosomal compartment. (**a**) cWAFs express higher LAMP1, LAMP2, and GLB1 levels. Abundance changes of proteins (SILAC ratio) indicate a significantly increased occurrence of LAMP1, LAMP2, and GLB1 in cWAFs (SILAC ratio is normalized to the values of NHFs; two-tailed, unpaired *t*-test; $*P < 0.05$, $***P < 0.001$). (**b**) Immunofluorescence staining of LAMP1. NHF2 and cWAF1 were stained with DAPI (blue) and an anti-LAMP1 antibody (green). cWAFs exhibit an enlarged lysosomal compartment. Bar = 100 μm. (**c**) Autophagy flux analysis. To analyze lysosomal activity, autophagy flux was analyzed in basal (DMEM) and starvation conditions (HBSS). Two NHFs were compared with two cWAFs, the latter consistently responding less to ConA treatment under basal conditions (DMEM). Bar diagram shows relative quantification of biological replicates (n = 6); $*P < 0.05$, two-tailed, unpaired *t*-test. ConA, concanamycin A; cWAF, chronic wound–associated fibroblast; HBSS, Hank's Balanced Salt Solution; NHF, normal human fibroblast; SILAC, stable isotope labeling by amino acids in cell culture.

probably a result of dysregulation of multiple joint and complementary mechanisms.

Increased abundance of adhesion complexes and reduced migration of cWAFs

Many integrins were profoundly enriched in cWAFs (Figure 4a and b). Integrin heterodimers αVβ1 and αVβ5 are responsible for activation of latent TGFβ1 and 3 (Dietz, 2015; Reed et al., 2015), mediate cell-matrix adhesion, and support migration. In addition to elevated integrin abundance, dysregulation of multiple other proteins known to stimulate wound healing such as transglutaminase 2, the second most upregulated protein in cWAFs (Table 2), and serpin H1/HSP47 (Eckert et al., 2014; Wang and Li, 2009) also pointed to an increased propensity for migration of cWAFs (Supplementary Figure S2). As this is in stark contrast to the observed clinical phenotype of decreased wound healing propensity and migration of cWAFs, we directly addressed the migratory ability of cWAFs in a functional assay. Confluent cell monolayers were wounded with a pipet tip and the closure of the scratch observed over time. In this assay, in accordance with previous findings (Brem et al., 2007; Wall et al., 2008), cWAFs possessed a significantly hampered wound closure potential compared with NHFs, which was likely a composite effect of slower migration and reduced proliferative capacity (Figure 4c and d, Figure 5a). These functional data together with the proteomics data indicate that cell-intrinsic changes in cWAFs lower the ability of these cells to migrate. An increased abundance of integrins at the plasma membrane of cWAFs may contribute to the incapacity of chronic wounds to close and to achieve dermal healing.

cWAFs exhibit impaired proliferation

Under steady-state conditions, proliferation of dermal fibroblasts in the adult body is rare. However, after wounding, the capacity of mesenchymal cells to increase proliferation is central for tissue repair (Driskell and Watt, 2015). Downregulation of growth factor receptors suggested that this process could be affected in cWAFs (Supplementary Figure S2) (Brem et al., 2007). Indeed, cell proliferation assays demonstrated a significantly lower proliferation of cWAFs as compared with NHFs (Figure 5a). In agreement with the cell biological phenotype, cWAFs exhibited depletion of all subunits of the hexameric DNA replication licensing factors MCM complex (Figure 5b), as demonstrated by western blot for MCM6 and MCM7 (Figure 5c). This was not only observed in vitro in cell culture but was also observed in skin sections in vivo (Figure 5d), indicating an inability of cWAFs to initiate genome replication, thus impairing cell proliferation.

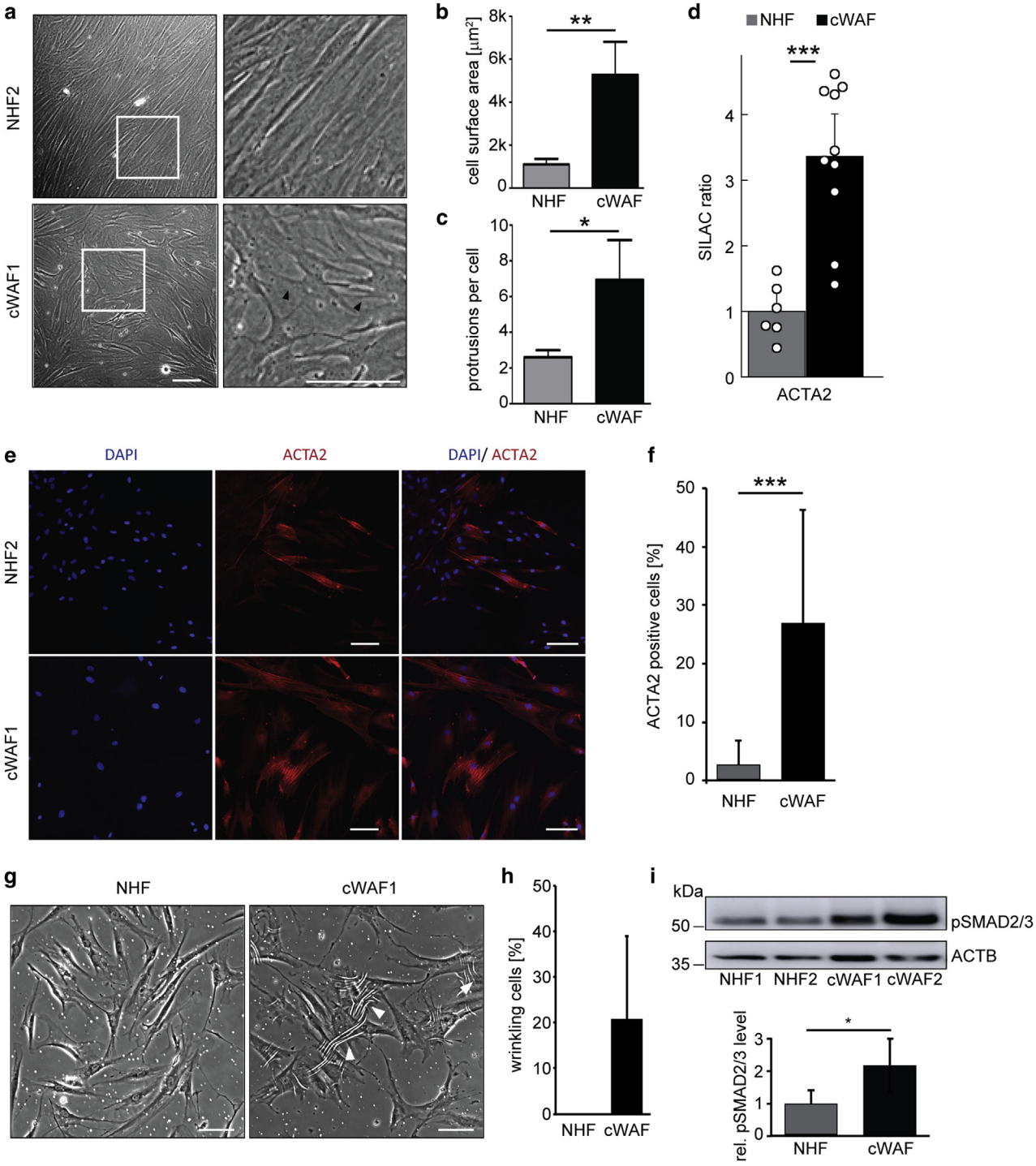

Figure 3. cWAFs exhibit enhanced contractile ability compared with NHFs. (**a**) Morphological differences between NHFs and cWAFs. Representative transmitted light micrographs of NHF2 and cWAF1. cWAFs are increased in size and show protrusions (black arrow heads). Right panels: magnification of white frame marked in left panels. Bar = 100 µm. (**b**) Quantification of cell surface area (n = 3 NHF and cWAF donors, 10 images per donor). (**c**) Quantification of protrusions per cell (n = 3 NHF and cWAF donors, 10 images per donor). (**d**) Increased protein abundance of ACTA2. MS-based proteomics analysis identified a significantly increased protein abundance of ACTA2 in cWAFs (two-tailed, unpaired *t*-test; ***$P < 0.001$). (**e**) Immunofluorescence analysis of ACTA2. ACTA2 was more abundant in cWAFs. Bar = 100 µm. (**f**) Quantification of ACTA2-positive cells. ACTA2-positive cells were counted in immunofluorescence micrographs as shown in panel (e). (**g**) Phase-contrast pictures of cells seeded on deformable fibronectin-coated silicone substrates. More wrinkles indicating matrix contraction are seen in cWAF cultures (marked by white arrowheads). Bar = 100 µm. (**h**) Quantification of wrinkling cells. An increased number of wrinkling cells can be seen for all cWAFs. No wrinkles were observed for NHFs, which represents an average of four different NHF populations. (**i**) Increased TGFβ activity in cWAFs. TGFβ activity was assessed by western blot detecting, phospho-Ser465/467 of SMAD2 and phospho-Ser423/425 of SMAD3. Shown are values normalized to actin/tubulin (n = 4). *$P < 0.05$, **$P < 0.01$, ***$P < 0.001$, two-tailed, unpaired *t*-test. cWAF, chronic wound–associated fibroblast; NHF, normal human fibroblast.

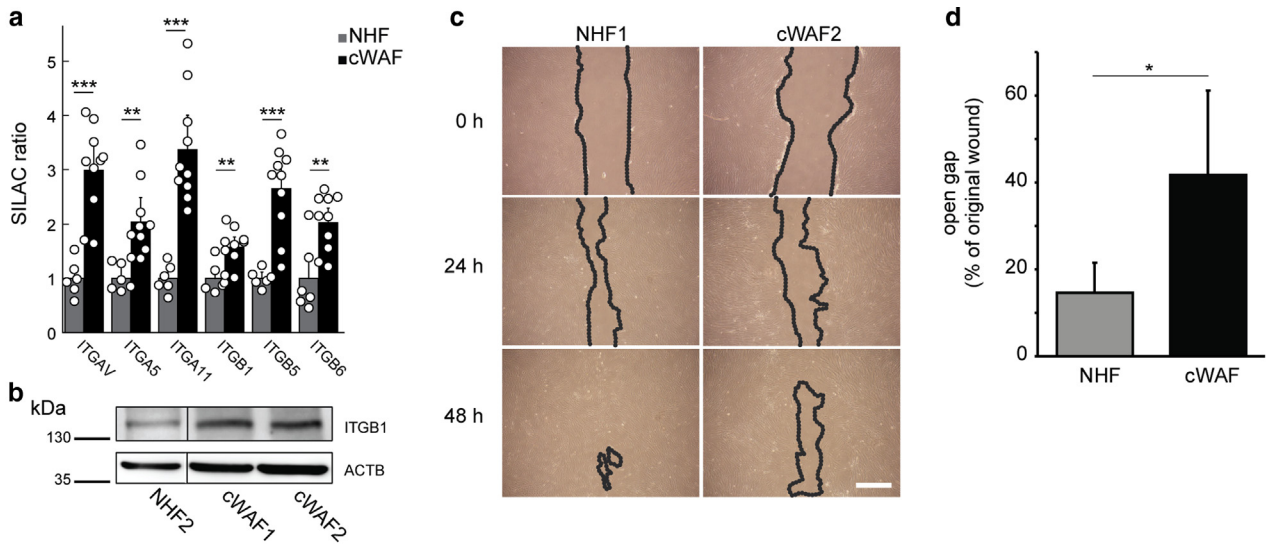

Figure 4. cWAFs show a decreased migration and increased abundances of adhesion molecules. (**a**) Integrins are enriched in cWAFs. Proteomics analysis identifies integrins ITGAV, ITGA5, ITGA11, ITGB1, ITGB5, and ITGB6 as significantly increased for cWAFs compared with NHFs (normalized to NHFs). (**b**) Increased ITGB1 abundance in cWAFs. The increased abundance of ITGB1 is confirmed by western blot. (**c**) cWAFs migrate slower than NHFs. Migration assay of NHF1 and cWAF2. Pictures were taken up to 48 hours after scratch; representative pictures are shown. Gap is closed after 48 hours by NHF. Bar = 200 μm. (**d**) Quantification of micrographs shown in (c) (n = 3 NHF and cWAF donors). $*P < 0.05$, $**P < 0.01$, $***P < 0.001$, two-tailed, unpaired *t*-test. cWAF, chronic wound–associated fibroblast; NHF, normal human fibroblast.

Pharmacological interference partially reverts cWAF phenotypes

cWAFs appear to occur as consequence of a chronically injured and inflamed microenvironment, potentially involving epigenetic changes, such as DNA methylation, which could lead to gene silencing and underlie decreased proliferation of cWAFs. To test this hypothesis, we aimed at reverting cWAFs pharmacologically, employing 5-azacytidine (5-aza), an inhibitor of DNA methyltransferases (Quintás-Cardama et al., 2010), concomitantly to interfering with the proinflammatory Janus kinase–STAT signaling pathway using the Janus kinase 1/2 inhibitor ruxolitinib (ruxo), as previously tested for cancer-associated fibroblasts (Albrengues et al., 2015; Damsky and King, 2017). The cells were singly or dually treated with the agents for one week and monitored for an additional two weeks in culture before analysis. Ruxo alone and combined with 5-aza increased expression of MCM7 in cWAFs, which was mirrored by an increase in cell proliferation (Figure 5e and f). Ruxo, 5-aza, or the combination of both reagents reduced the abundance of alpha smooth muscle actin (Figure 5g), which was functionally mirrored by the lesser ability of cWAFs to contract free-floating collagen lattices (Figure 5h). Collectively, only the combination of ruxo and 5-aza was able to increase MCM7 abundance and cell proliferation and to reduce alpha smooth muscle actin. This suggests that, for best and most sustained reversion, combined targeting of the Janus kinase–STAT pathway and DNA methylation is needed. Taken together, the data indicate that cWAFs are not terminally modified and that pharmacological intervention may be able to revert the cWAF phenotype.

DISCUSSION

It is becoming increasingly evident that dermal fibroblasts are not a homogenous group of cells but are heterogeneous by both ontology and function (Driskell et al., 2013; Driskell and Watt, 2015; Nauroy et al., 2017). In this study, we compared the proteomes of NHFs, aWAFs, and myofibroblasts with that of cWAFs. Cells were metabolically labeled for two weeks before proteome analyses, and we cannot formally exclude alterations owing to culture conditions. However, as we have shown in the past that proteomes of primary NHFs were relatively stable for up to 14 passages (Sprenger et al., 2010), and as we could discriminate cells based on their proteome profiles in this study, we are confident that the observed proteomic differences to a large extent reflect in vivo alterations. Similarities between aWAFs, NHFs, and myofibroblasts were expected given that activation of fibroblasts occurs during standard cell culture (Baranyi et al., 2019; Iyer et al., 1999). However, cWAFs were disparately different to aWAFs, NHFs, and myofibroblasts, displaying a distinct phenotype with acquired cell-intrinsic changes not supportive of tissue repair. Whereas cWAFs showed partial similarities with the other cell types, they were clearly discriminable by their proteomic signature, that is, by the high abundance of TGM2.

So far, wound healing therapies have mainly aimed at achieving epidermal coverage. Consequently, significant focus has been placed on understanding processes regulating re-epithelialization (Martin and Nunan, 2015). However, it is apparent that pathological changes of mesenchymal-derived cells contribute to regulation of re-epithelialization and wound healing disorders, as well (Brem et al., 2007; Hiebert et al., 2018; Wall et al., 2008). These cells are understudied and not well characterized in the context of chronic wounds. Here, we aimed to better understand the distinct molecular characteristics that separate cWAFs from fibroblasts able to support tissue repair. Our proteome analyses revealed two major groups of dysregulated processes in cWAFs compared with NHFs. The first relates to processes linked to lysosomal

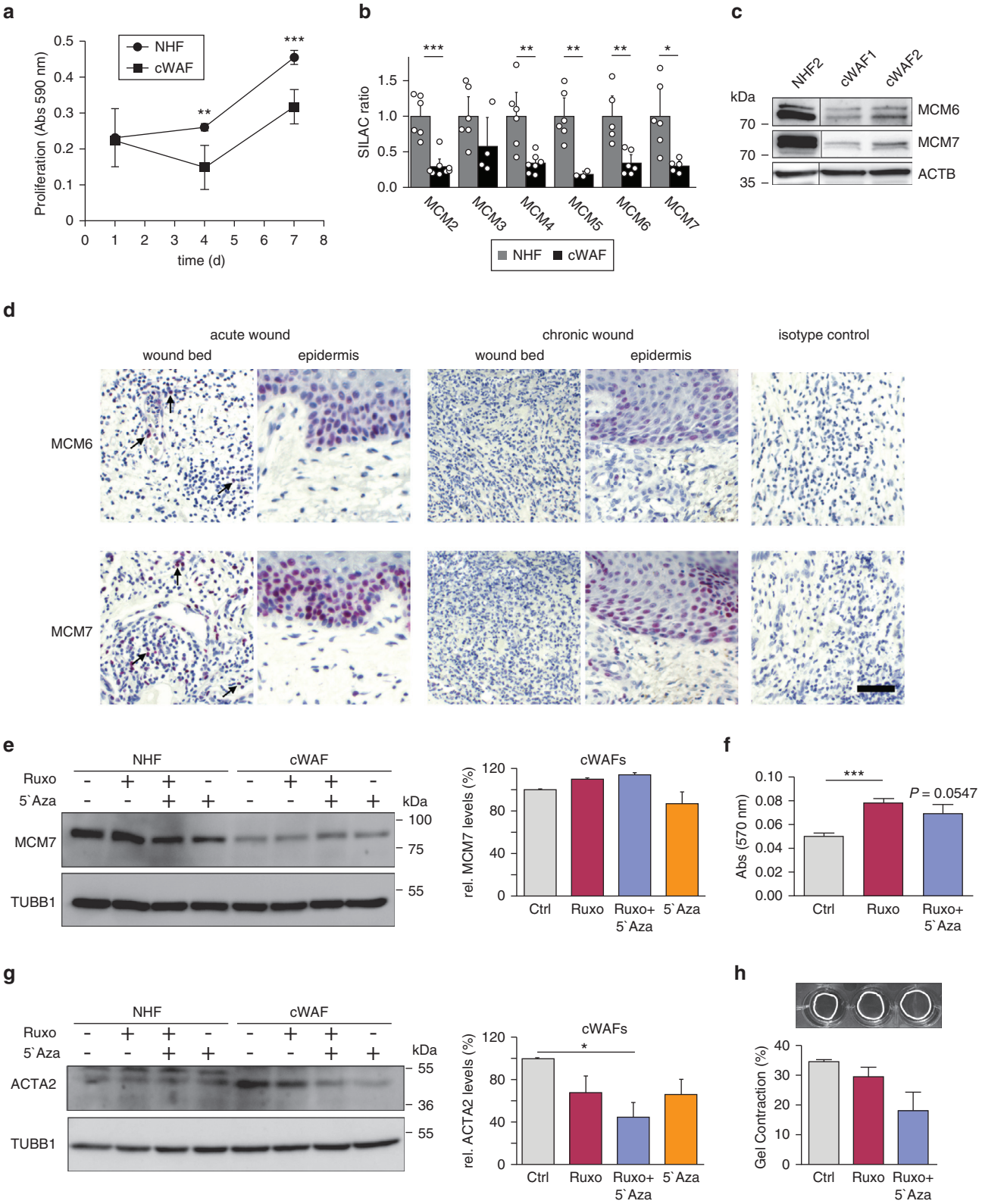

Figure 5. Proliferation is diminished and MCM proteins are reduced in cWAFs. (**a**) Proliferation assay. Proliferation is measured by relative absorbance at 590 nm over seven days. After seven days, cWAFs are less dense than NHFs (n = 3 NHF and cWAF donors). (**b**) MCM subunits are reduced in cWAFs. Protein abundances of all subunits of the MCM complex were significantly decreased in cWAFs compared with NHFs (unpaired two-tailed *t*-test, Welch corrected; $*P < 0.05$, $**P < 0.01$, $***P < 0.001$). (**c**) Reduced abundance of MCM6 and MCM7. Reduced protein abundance of MCM6 and 7 in cWAFs as detected by LC-MS/MS was confirmed by western blot. (**d**) Reduced abundance of MCM6 and MCM7 in the dermis of chronic wounds. Sections of acute and chronic human wounds stained for MCM6 and MCM7. In the wound bed of acute wounds, MCM6 and MCM7 are increased (arrows). This increase is almost completely absent in chronic wounds. Bar = 50 µm. (**e**–**h**) Combined ruxo and 5-aza treatment partially reverts cWAFs. NHFs or cWAFs were treated with ruxo and 5-aza alone or in combination for one week and maintained for an additional two weeks in culture before analysis. (e) Representative western blot and quantification for

capacity and protein turnover, cWAFs exhibiting potentially age-associated dysfunctions, such as altered distribution, abundance, and activity of lysosomes (Dumit et al., 2014). Control cells were from age-matched individuals, implying that the aged phenotype of cWAFs is primarily dependent on factors others than the donors' age. Expansion of the lysosomal compartment and lysosomal dysfunction is seen in many diseases connected to aging, such as Parkinson and Alzheimer diseases (Cellerino and Ori, 2017). The increase in lysosomal mass might also indicate a senescence-associated secretory phenotype. This might (i) contribute to an increased release of lysosomal proteinases into the extracellular space, thus promoting a tissue damage milieu, which has been suggested to contribute to the inability of chronic wounds to heal (Kirsner et al., 2015; Yager and Nwomeh, 1999), and (ii) boost production and release of proinflammatory cytokines (Freund et al., 2010). In addition, the senescent phenotype implies that cWAFs represent a cellular phenotype beyond repair. Although we partially succeeded in stimulating cell proliferation by blocking Janus kinase–STAT signaling and DNA methyltransferases, outlining potential treatment strategies, cell reversion was only partial as cWAFs could still be discriminated morphologically and biologically from NHFs, proliferating less than the latter.

Increased smooth muscle actin and integrin abundance indicated the second dysregulated process in cWAFs that stood out: increased TGFβ activity. Altered TGFβ activity is commonly seen in wound healing pathologies. Depending on the wound subtype, decreased (Cooper et al., 1994) or increased (Nyström et al., 2015) activities have been reported. The fact that TGFβ activity is indeed enhanced in situ in chronic wounds is reflected by the fibrotic wound edges that occur in well-perfused chronic wounds. Although elevated TGFβ activity is a general feature of isolated cWAFs, the cells are unable to close dermal wounds in vivo. This suggests that elevated TGFβ activity alone, reflected by an increased ECM contraction capacity of cWAFs, is not enough to support wound closure. It appears that the inability of cWAFs to do so is due to a composite of effects, which involve reduced proliferative and migratory abilities.

More research is needed to address the therapeutic potential of pharmacological intervention to correct cWAF functions. One relevant question in this context is whether the increased proliferative and reduced contractile capacity of cWAFs after ruxo and 5-aza treatment is therapeutically meaningful in vivo in a chronic wound. An additional and potentially more efficacious strategy promoting wound healing would be enforced rejuvenation of the fibroblasts surrounding the wounded tissue by targeted removal of cWAFs. Such a strategy was successfully employed in a mouse model of scleroderma (Lagares et al., 2017). To eliminate myofibroblasts in fibrotic tissue, cell death was induced in a cell type–specific manner by targeting apoptosis-primed mitochondria.

Our data support the notion that therapies targeting TGFβ may have only limited benefit for treatment of chronic wounds (Han and Ceilley, 2017). In line with elevated TGFβ signaling, the TGFβ-stimulating integrin subunits αV, β1, and β5 were significantly upregulated in cWAFs when compared with NHFs. It is very likely that, next to promoting TGFβ signaling, increased integrin abundance regulates cell adhesion and migration of cWAFs (Liu et al., 2010).

Taken together, cWAFs can be considered as a distinct cell phenotype and could be a prime target for future wound healing therapies using biologically and/or pharmacologically active compounds that, alone or in combination, can revert their regeneration-averse phenotype. The medical and socioeconomic impact of such therapeutic regimens would be enormous.

MATERIALS AND METHODS

Additional Materials and Methods can be found online as supplementary information.

Patients and diagnosis

Skin specimens were obtained from five patients with chronic leg ulcers because of venous insufficiency or after trauma (cWAF1–5) for diagnostic purposes after written informed consent. To elucidate disease mechanisms, cWAFs were compared with NHF1–6 derived from age-matched healthy donors (Table 1). Cells used for each experiment are indicated in the respective figure according to the designations introduced in Table 1. Pictures were taken to illustrate clinical phenotypes of chronic leg ulcers. Transmitted light micrographs visualize differences between NHFs and cWAFs. The study was approved by the Ethics Committee of Freiburg University (# 521/13) and conducted according to the Declaration of Helsinki.

Cell culture and stable isotope labeling by amino acids in cell culture

Fibroblasts were isolated nonenzymatically from skin samples of the five patients and, as controls, from the skin of six healthy, age-matched controls as described previously (Sprenger et al., 2013). Cells were subcultured and passaged in DMEM (Gibco, Thermo Fisher Scientific, Waltham, MA), supplemented with fetal bovine serum gold (PAA, GE Healthcare, Chicago, IL) and penicillin/streptomycin (PAN-Biotech, Aidenbach, Germany). For mass spectrometry (MS) analysis, cells were cultured in stable isotope labeling by amino acids in cell culture–DMEM (PAN-Biotech) essentially as described previously (Küttner et al., 2014).

MS sample preparation and analysis

Samples were heated in SDS-PAGE loading buffer, reduced with 1 mM DTT for 10 minutes at 95 °C, and alkylated using 5.5 mM iodoacetamide for 30 minutes at room temperature. Protein mixtures were separated on 4–12% gradient gels, and proteins were in-gel digested with trypsin (Rappsilber et al., 2007). MS measurements were performed on an LTQ Orbitrap XL mass spectrometer coupled

MCM7. β-tubulin (TUBB1) was used to ensure equal loading (n = 2). (f) MTT proliferation assays of cWAFs two weeks after ruxo, ruxo and 5-aza, or no treatment (Ctrl). Values represent mean ± SEM, n = 4, ***$P < 0.001$. (g) Representative western blot and quantification for alpha smooth muscle actin (ACTA2); TUBB1 was used to ensure equal loading (n = 6). (h) Photos of cWAF-populated free-floating collagen lattices 24 hours after release of the gels. Cells received treatment with 5-aza and/or ruxo for one week and were cultured for an additional two weeks before analysis. White lines indicate the edges of the gel. Values represent mean ± SEM, n = 2 of different cWAF donors. 5-aza, 5-azacytidine; cWAF, chronic wound–associated fibroblast; LC, liquid chromatography; NHF, normal human fibroblast; ruxo, ruxolitinib.

to an Agilent 1200 nanoflow−HPLC. HPLC column tips (fused silica) with 75-μm inner diameter were self-packed with Reprosil−Pur 120 ODS−3 to a length of 20 cm. The mass spectrometer was operated in the data-dependent mode and switched automatically between MS and maximally five MS/MS scans.

Data availability statement

The mass spectrometry proteomics data are publicly available and have been deposited to the ProteomeXchange Consortium via the PRIDE partner repository with the dataset identifier PXD005873 (Vizcaíno et al., 2016).

ORCIDs

Bettina Berberich: http://orcid.org/0000-0001-6891-7235
Kerstin Thriene: http://orcid.org/0000-0002-7642-5078
Christine Gretzmeier: http://orcid.org/0000-0003-3949-8531
Tobias Kühl: http://orcid.org/0000-0002-6682-2096
Hans Bayer: http://orcid.org/0000-0002-1061-4298
Ioannis Athanasiou: http://orcid.org/0000-0002-5158-673X
David Ali Rafei-Shamsabadi: http://orcid.org/0000-0002-7850-3199
Leena Bruckner-Tuderman: http://orcid.org/0000-0001-8339-9093
Alexander Nyström: http://orcid.org/0000-0002-4666-2240
Dimitra Kiritsi: http://orcid.org/0000-0002-2331-8981
Jörn Dengjel: http://orcid.org/0000-0002-9453-4614

CONFLICT OF INTEREST

The authors state no conflict of interest.

ACKNOWLEDGMENTS

The authors thank Boris Hinz, University of Toronto for providing deformable silicone substrates for the wrinkling assays. This work was supported by the German Research Foundation (DFG) through DE 1757/3-2 (JD), NY90/2-1, NY90/3-2, NY90/5-1 and SFB850 project B11 (AN), and KI1795/1-1, KI 1795/2-1 (DK), the Swiss National Science Foundation and the canton of Fribourg (JD), and a research grant from the Dystrophic Epidermolysis Bullosa Research Association Nyström-Bruckner-Tuderman 1 (LBT, AN).

AUTHOR CONTRIBUTIONS

Conceptualization: AN, DK, JD; Data Curation: AN, DK, JD; Funding Acquisition: LBT, AN, DK, JD; Investigation: BB, KT, CG, TK, HB, IA, DRS; Project Administration: LBT, AN, DK, JD; Writing - Original Draft Preparation: BB, KT, LBT, AN, DK, JD; Writing - Review and Editing: BB, KT, CG, TK, HB, IA, DRS, LBT, AN, DK, JD

SUPPLEMENTARY MATERIAL

Supplementary material is linked to the online version of the paper at www.jidonline.org, and at https://doi.org/10.1016/j.jid.2020.02.040.

REFERENCES

Albrengues J, Bertero T, Grasset E, Bonan S, Maiel M, Bourget I, et al. Epigenetic switch drives the conversion of fibroblasts into proinvasive cancer-associated fibroblasts. Nat Commun 2015;6:10204.

Baranyi U, Winter B, Gugerell A, Hegedus B, Brostjan C, Laufer G, et al. Primary human fibroblasts in culture switch to a myofibroblast-like phenotype independently of TGF beta. Cells 2019;8:721.

Bizet AA, Liu K, Tran-Khanh N, Saksena A, Vorstenbosch J, Finnson KW, et al. The TGF-beta co-receptor, CD109, promotes internalization and degradation of TGF-beta receptors. Biochim Biophys Acta 2011;1813:742−53.

Brem H, Stojadinovic O, Diegelmann RF, Entero H, Lee B, Pastar I, et al. Molecular markers in patients with chronic wounds to guide surgical debridement. Mol Med 2007;13:30−9.

Cellerino A, Ori A. What have we learned on aging from omics studies? Semin Cell Dev Biol 2017;70:177−89.

Cha J, Kwak T, Butmarc J, Kim TA, Yufit T, Carson P, et al. Fibroblasts from non-healing human chronic wounds show decreased expression of beta ig-h3, a TGF-beta inducible protein. J Dermatol Sci 2008;50:15−23.

Charles CA, Tomic-Canic M, Vincek V, Nassiri M, Stojadinovic O, Eaglstein WH, et al. A gene signature of nonhealing venous ulcers: potential diagnostic markers. J Am Acad Dermatol 2008;59:758−71.

Chester D, Brown AC. The role of biophysical properties of provisional matrix proteins in wound repair. Matrix Biol 2017;60−61:124−40.

Cooper DM, Yu EZ, Hennessey P, Ko F, Robson MC. Determination of endogenous cytokines in chronic wounds. Ann Surg 1994;219:688−91: [discussion 91−2].

Damsky W, King BA. JAK inhibitors in dermatology: the promise of a new drug class. J Am Acad Dermatol 2017;76:736−44.

Desmoulière A, Geinoz A, Gabbiani F, Gabbiani G. Transforming growth factor-beta 1 induces alpha-smooth muscle actin expression in granulation tissue myofibroblasts and in quiescent and growing cultured fibroblasts. J Cell Biol 1993;122:103−11.

Dietz HC. One integrin to rule them all? Sci Transl Med 2015;7:288fs21.

Dörr JR, Yu Y, Milanovic M, Beuster G, Zasada C, Däbritz JH, et al. Synthetic lethal metabolic targeting of cellular senescence in cancer therapy. Nature 2013;501:421−5.

Driskell RR, Lichtenberger BM, Hoste E, Kretzschmar K, Simons BD, Charalambous M, et al. Distinct fibroblast lineages determine dermal architecture in skin development and repair. Nature 2013;504:277−81.

Driskell RR, Watt FM. Understanding fibroblast heterogeneity in the skin. Trends Cell Biol 2015;25:92−9.

Dumit VI, Küttner V, Käppler J, Piera-Velazquez S, Jimenez SA, Bruckner-Tuderman L, et al. Altered MCM protein levels and autophagic flux in aged and systemic sclerosis dermal fibroblasts. J Invest Dermatol 2014;134:2321−30.

Eckert RL, Kaartinen MT, Nurminskaya M, Belkin AM, Colak G, Johnson GV, et al. Transglutaminase regulation of cell function. Physiol Rev 2014;94:383−417.

Eming SA, Martin P, Tomic-Canic M. Wound repair and regeneration: mechanisms, signaling, and translation. Sci Transl Med 2014;6:265sr6.

Freund A, Orjalo AV, Desprez PY, Campisi J. Inflammatory networks during cellular senescence: causes and consequences. Trends Mol Med 2010;16:238−46.

Geiger T, Cox J, Ostasiewicz P, Wisniewski JR, Mann M. Super-SILAC mix for quantitative proteomics of human tumor tissue. Nat Methods 2010;7:383−5.

Gurtner GC, Werner S, Barrandon Y, Longaker MT. Wound repair and regeneration. Nature 2008;453:314−21.

Han G, Ceilley R. Chronic wound healing: a review of current management and treatments. Adv Ther 2017;34:599−610.

Has C, Nyström A. Epidermal basement membrane in health and disease. Curr Top Membr 2015;76:117−70.

Hiebert P, Wietecha MS, Cangkrama M, Haertel E, Mavrogonatou E, Stumpe M, et al. Nrf2-mediated fibroblast reprogramming drives cellular senescence by targeting the matrisome. Dev Cell 2018;46:145−61.e10.

Hinz B. The extracellular matrix and transforming growth factor-beta1: tale of a strained relationship. Matrix Biol 2015;47:54−65.

Iyer VR, Eisen MB, Ross DT, Schuler G, Moore T, Lee JC, et al. The transcriptional program in the response of human fibroblasts to serum. Science 1999;283:83−7.

Kilpatrick BS, Magalhaes J, Beavan MS, McNeill A, Gegg ME, Cleeter MW, et al. Endoplasmic reticulum and lysosomal Ca^{2+} stores are remodelled in GBA1-linked Parkinson disease patient fibroblasts. Cell Calcium 2016;59:12−20.

Kiritsi D, Nyström A. The role of TGFbeta in wound healing pathologies. Mech Ageing Dev 2018;172:51−8.

Kirsner RS, Baquerizo Nole KL, Fox JD, Liu SN. Healing refractory venous ulcers: new treatments offer hope. J Invest Dermatol 2015;135:19−23.

Küttner V, Mack C, Gretzmeier C, Bruckner-Tuderman L, Dengjel J. Loss of collagen VII is associated with reduced transglutaminase 2 abundance and activity. J Invest Dermatol 2014;134:2381−9.

Küttner V, Mack C, Rigbolt KT, Kern JS, Schilling O, Busch H, et al. Global remodelling of cellular microenvironment due to loss of collagen VII. Mol Syst Biol 2013;9:657.

Lagares D, Santos A, Grasberger PE, Liu F, Probst CK, Rahimi RA, et al. Targeted apoptosis of myofibroblasts with the BH3 mimetic ABT-263 reverses established fibrosis. Sci Transl Med 2017;9:eaal3765.

Lee BY, Han JA, Im JS, Morrone A, Johung K, Goodwin EC, et al. Senescence-associated beta-galactosidase is lysosomal beta-galactosidase. Aging Cell 2006;5:187−95.

Liu S, Xu SW, Blumbach K, Eastwood M, Denton CP, Eckes B, et al. Expression of integrin beta 1 by fibroblasts is required for tissue repair in vivo. J Cell Sci 2010;123:3674–82.

Martin P, Nunan R. Cellular and molecular mechanisms of repair in acute and chronic wound healing. Br J Dermatol 2015;173:370–8.

Murphy-Ullrich JE, Downs JC. The Thrombospondin1-TGF-beta pathway and glaucoma. J Ocul Pharmacol Ther 2015;31:371–5.

Nagaraja S, Wallqvist A, Reifman J, Mitrophanov AY. Computational approach to characterize causative factors and molecular indicators of chronic wound inflammation. J Immunol 2014;192:1824–34.

Nauroy P, Barruche V, Marchand L, Nindorera-Badara S, Bordes S, Closs B, et al. Human dermal fibroblast subpopulations display distinct gene signatures related to cell behaviors and matrisome. J Invest Dermatol 2017;137:1787–9.

Nyström A, Thriene K, Mittapalli V, Kern JS, Kiritsi D, Dengjel J, et al. Losartan ameliorates dystrophic epidermolysis bullosa and uncovers new disease mechanisms. EMBO Mol Med 2015;7:1211–28.

Pakshir P, Hinz B. The big five in fibrosis: macrophages, myofibroblasts, matrix, mechanics, and miscommunication. Matrix Biol 2018;68–69:81–93.

Pang C, Ibrahim A, Bulstrode NW, Ferretti P. An overview of the therapeutic potential of regenerative medicine in cutaneous wound healing. Int Wound J 2017;14:450–9.

Quintás-Cardama A, Santos FP, Garcia-Manero G. Therapy with azanucleosides for myelodysplastic syndromes. Nat Rev Clin Oncol 2010;7:433–44.

Rappsilber J, Mann M, Ishihama Y. Protocol for micro-purification, enrichment, pre-fractionation and storage of peptides for proteomics using StageTips. Nat Protoc 2007;2:1896–906.

Reed NI, Jo H, Chen C, Tsujino K, Arnold TD, DeGrado WF, et al. The αvβ1 integrin plays a critical in vivo role in tissue fibrosis. Sci Transl Med 2015;7:288ra79.

Schäfer M, Werner S. Cancer as an overhealing wound: an old hypothesis revisited. Nat Rev Mol Cell Biol 2008;9:628–38.

Shaw TJ, Martin P. Wound repair: a showcase for cell plasticity and migration. Curr Opin Cell Biol 2016;42:29–37.

Sprenger A, Küttner V, Biniossek ML, Gretzmeier C, Boerries M, Mack C, et al. Comparative quantitation of proteome alterations induced by aging or immortalization in primary human fibroblasts and keratinocytes for clinical applications. Mol Biosyst 2010;6:1579–82.

Sprenger A, Küttner V, Bruckner-Tuderman L, Dengjel J. Global proteome analyses of SILAC-labeled skin cells. Methods Mol Biol 2013;961:179–91.

Tabib T, Morse C, Wang T, Chen W, Lafyatis R. SFRP2/DPP4 and FMO1/LSP1 define major fibroblast populations in human skin. J Invest Dermatol 2018;138:802–10.

Vizcaíno JA, Csordas A, del-Toro N, Dianes JA, Griss J, Lavidas I, et al. 2016 update of the PRIDE database and its related tools. Nucleic Acids Res 2016;44:D447–56.

Wall IB, Moseley R, Baird DM, Kipling D, Giles P, Laffafian I, et al. Fibroblast dysfunction is a key factor in the non-healing of chronic venous leg ulcers. J Invest Dermatol 2008;128:2526–40.

Wang Z, Li L. The plasmid encoding HSP47 enhances collagen expression and promotes skin wound healing in an alloxan-induced diabetic model. Cell Biol Int 2009;33:705–10.

Widgerow AD. Chronic wounds - is cellular 'reception' at fault? Examining integrins and intracellular signalling. Int Wound J 2013;10:185–92.

Yager DR, Nwomeh BC. The proteolytic environment of chronic wounds. Wound Repair Regen 1999;7:433–41.

SUPPLEMENTARY MATERIALS AND METHODS

Experimental design and statistical rationale

In total, we analyzed 11 primary cell populations as listed in Table 1. Proteomics analyses were performed from five primary chronic wound–associated fibroblast and two primary normal human fibroblasts populations. For stable isotope labeling by amino acids in cell culture–based proteomics analyses, two biological replicates each were analyzed using swapped labels. All statistical tests were corrected for multiple testing as outlined in the respective paragraphs.

Cell culture and stable isotope labeling by amino acids in cell culture

Fibroblasts were isolated from skin samples of the five patients and, as controls, from the skin of six healthy, age-matched controls. Cells were subcultured and passaged in DMEM (Gibco, Thermo Fisher Scientific, Waltham, MA), supplemented with fetal bovine serum gold (PAA, GE Healthcare, Chicago, IL) and penicillin/streptomycin (PAN-Biotech, Aidenbach, Germany).

The model of myofibroblasts was achieved by culturing normal human fibroblasts at low density (5 cells/mm^2), and the medium was supplemented with 2 ng/ml TGFβ1 (Peprotech, Rocky Hill, NJ) for seven days.

Cells were harvested with 1 ml of 1x DPBS (PAN-Biotech) containing complete protease inhibitor cocktail (Roche, Basel, Switzerland) by scraping and centrifuging at 300*g*. Cell pellets were incubated with lysis buffer (25 mM Tris-HCl pH 7.5, 0.1 M NaCl, 1% NP-40, EDTA, Pefablock, Phosphatase inhibitor 3 cocktail, PHJ2) on a shaker for 20 minutes on ice and centrifuged at 13,000 rpm for 10 minutes. Supernatants were incubated for 10 minutes at 95 °C in SDS buffer and directly used for western blot analysis or stored at −80 °C until use.

For MS analysis, cells were cultured in in stable isotope labeling by amino acids in cell culture–DMEM (PAN-Biotech) essentially as described (Küttner et al., 2014). Stable isotope labeling by amino acids in cell culture–DMEM was supplemented with dialyzed fetal bovine serum (Life Technologies, Carlsbad, CA), penicillin/streptomycin (PAN-Biotech), 82 mg/liter proline, 42 mg/liter L-arginine, and 73 mg/liter L-lysine for the unlabeled condition. Cells were heavy-labeled for 2 weeks with 82 mg/liter proline, 42 mg/liter L-arginine-$^{13}C_6$-$^{15}N_4$ (Arg_{10}), and 73 mg/liter L-lysine-$^{13}C_6$-$^{15}N_2$ (Lys_8) or medium-labeled with 82 mg/liter proline, 42 mg/liter L-arginine-$^{13}C_6$ (Arg_6), and 73 mg/liter L-lysine-$^{2}H_4$ (Lys_4). Biological replicates were obtained by swapping labels. Cell pellets were solely lysed by direct incubation for 10 minutes at 95 °C in SDS buffer.

Chronic wound–associated fibroblasts were treated with 5 μM ruxolitinib (Jakavi, Novartis, Basel, Switzerland) dissolved in DMSO and 10 μM 5-azacitidine (Sigma, St. Louis, MO) daily for one week, as previously described (Albrengues et al., 2015).

Western blot

Cell lysates were separated by SDS-PAGE using self-casted SDS gels and transferred onto nitrocellulose membranes. Membranes were blocked with 5% milk powder in 1x TBS-T for a minimum of 1 hour at room temperature and incubated with primary antibodies diluted with the same buffer overnight at 4 °C. Horseradish peroxidase–conjugated secondary antibodies and a chemiluminescent detection assay (Immobilon Western, Millipore, Burlington, MA) were used for visualization according to manufacturer's instructions.

To quantify changes of protein amounts, the samples were quantified using Image J Intensities (AU) and intensities normalized to the β-actin signals from the same blots. The following antibodies were used for western blot analysis: anti–β-actin (C4, sc-47778), 1:1,000; anti–MCM6 (B-4, sc-55576), 1:1,000; anti-MCM7 (0.N.194, sc-71550), 1:1,000; anti-TGM2 (sc-48387), 1:1,000 (all Santa Cruz Biotechnology, Dallas, TX); anti–phospho-Smad3 (phospho S423 + S425; EP823Y; ab52903, Abcam, Cambridge, United Kingdom), 1:1,000; anti–phospho-Smad2 (Ser465/467 (138D4) Cell Signaling Technology, Danvers, MA), 1:1,000; and anti-ITGB1 (MAB1965, Merck, Kenilworth, NJ), 1:1,000.

MS sample preparation

Samples were heated in SDS-PAGE loading buffer, reduced with 1 mM DTT for 10 minutes at 95 °C, and alkylated using 5.5 mM iodoacetamide for 30 minutes at room temperature. Protein mixtures were separated on 4–12% gradient gels. The gel lanes were cut into 10 equal slices, the proteins were in-gel digested with trypsin, and the resulting peptide mixtures were processed on STAGE tips and analyzed by liquid chromatography–MS/MS (Rappsilber et al., 2007).

Mass spectrometry

MS measurements were performed on an LTQ Orbitrap XL mass spectrometer coupled to an Agilent 1200 nano-flow–HPLC. HPLC column tips (fused silica) with 75-μm inner diameter were self-packed with Reprosil–Pur 120 ODS–3 to a length of 20 cm. Samples were applied directly onto the column without a precolumn. A gradient of A (0.5% acetic acid in water) and B (0.5% acetic acid in 80% acetonitrile in water) with increasing organic proportion was used for peptide separation (loading of sample with 2% B; separation ramp: from 10–30% B within 80 minutes). The flow rate was 250 nl/min and for sample application, 500 nl/min. The mass spectrometer was operated in the data-dependent mode and switched automatically between MS (maximum of 1×10^6 ions) and MS/MS. Each MS scan was followed by a maximum of five MS/MS scans in the linear ion trap using normalized collision energy of 35% and a target value of 5,000. Parent ions with a charge state from $z = 1$ and unassigned charge states were excluded for fragmentation. The mass range for MS was $m/z = 370–2,000$. The resolution was set to 60,000. MS parameters were as follows: spray voltage 2.3 kV; no sheath and auxiliary gas flow; ion-transfer tube temperature 125 °C.

Identification of proteins and protein ratio assignment using MaxQuant

The MS raw data files were uploaded into the MaxQuant software, version 1.4.1.2 for peak detection, generation of peak lists of mass error corrected peptides, and database searches (Cox and Mann, 2008). A full-length UniProt human database additionally containing common contaminants such as keratins and enzymes used for in-gel digestion (based on UniProt human FASTA, version August 2015) was used as reference. Carbamidomethylcysteine was set as fixed

modification, and protein amino-terminal acetylation and oxidation of methionine were set as variable modifications. Triple SILAC was chosen as quantitation mode. Three missed cleavages were allowed, enzyme specificity was trypsin/P, and the MS/MS tolerance was set to 0.5 Da. The average mass precision of identified peptides was in general less than 1 ppm after recalibration. Peptide lists were further used by MaxQuant to identify and relatively quantify proteins using the following parameters: peptide and protein false discovery rates, based on a forward-reverse database, were set to 0.01; minimum peptide length was set to 6; minimum number of peptides for identification and quantitation of proteins was set to one, which must be unique; minimum ratio count was set to two; and identified proteins were requantified. The 'match-between-run' option (2 minutes) was used.

The mass spectrometry proteomics data have been deposited to the ProteomeXchange Consortium via the PRIDE partner repository with the dataset identifier PXD005873 (Vizcaino et al., 2016).

Proteomics data analysis

Obtained data by MaxQuant 1.4.1.2 was analyzed with the freely available Perseus software (Tyanova et al., 2016). Data were $\log_2$ transformed and significance was tested with two-samples test with a false discovery rate according to Benjamini-Hochberg set to 0.05. For cluster analysis, protein ratios were z-normalized. Proteins in each hierarchical cluster were tested for enriched Gene Ontology terms (biological process and cellular compartment).

Immunostaining

Fibroblasts were grown on collagen I–coated coverslips for 2 days. Cells were fixed with 4% paraformaldehyde for 15 minutes, permeabilized with 0.1% Triton 100-X in Dulbecco's PBS (DPBS) for 5 minutes, and blocked with 2% BSA in DPBS for 30 minutes at room temperature. The primary antibody diluted with 1% BSA in DPBS was incubated 1 hour minimum at room temperature. After incubation with the secondary antibody diluted in 1% BSA in DPBS for 45 min, DPBS-washed slides were embedded in ProLong Gold DAPI overnight at room temperature. The primary antibodies were anti–LAMP-2 (sc-18822, Santa Cruz Biotechnology) and anti-ACTA2 (sc-53142, Santa Cruz, USA). Alexa 594- and Alexa 488-conjugated secondary antibodies (Invitrogen, Thermo Fisher Scientific) were used. Pictures were taken with an IF confocal microscope (Zeiss confocal microscopes, Zeiss, Oberkochen, Germany).

Human skin, acute wounds, and chronic wounds were stained with anti-MCM6 (B-4, sc-55576), 1:1,000, and anti-MCM7 (0.N.194, sc-71550) 1:1,000 after heat-mediated antigen retrieval.

Cell contraction assay

Cell contractility was assessed using deformable silicone substrates as has been described previously (Godbout et al., 2013). The 24-well plates were coated with 75 μl of silicone mixture with a defined stiffness of 5 kPa. The silicone substrates were coated with 10 μg/ml human fibronectin (Sigma-Aldrich). Cells were seeded at a concentration of 10,000 cells/cm^2, and wrinkle formation on substrates was observed after 24 hours in culture. Images were acquired via phase-contrast microscopy (Zeiss) and analyzed using ImageJ software (National Institutes of Health, Bethesda, MD). Relative contraction was expressed as number of cells associated with wrinkles to total amount of cells.

Collagen lattice contraction assays

Collagen lattice contraction assays were performed as previously described (Nyström et al., 2015). Chronic wound fibroblasts two weeks after treatment with ruxolitinib or ruxolitinib and 5-azacitidine as described previously were collected by trypsinization and resuspended in DMEM containing 0.1% fetal calf serum. The assay was performed in 12-well plates, and 250,000 cells in 1 ml of 0.4 mg/ml rat tail collagen and DMEM with 0.1% fetal calf serum were added per well. The solution was allowed to gel for 1 hour at 37 °C in a cell incubator with 5% CO_2. After this, 1 ml of DMEM containing 0.1% fetal calf serum was added and the plate was left in the cell incubator for an additional 2 hours, after which gels were released by a 200-μl pipet tip. Pictures were taken immediately after release of the gels and after 24 hours. Contraction of gels was quantified using Image J.

Cell migration assay

Fibroblasts were seeded onto collagen I–coated 60-mm dishes to create confluent monolayers. A scratch was introduced, and images were captured after 0 hours, 8 hours, 16 hours, 24 hours, and 48 hours with a transmitted light camera. Lines were introduced to highlight the remaining gaps.

Proliferation assay

For assessment of proliferation, equal numbers of fibroblasts were seeded on microplates with a local ionic electrode interface. At the indicated time points, the cells were stained by incubation with 3-(4,5-dimethylthiazol-2-yl)-2,5-diphenyltetrazolium bromide; subsequently, the detergent reagent was added to each well, and the cell numbers were quantified by measuring the absorbance at 570 nm on an Infinite 200 microtiter plate reader (Tecan, Zurich, Switzerland).

SUPPLEMENTARY REFERENCES

Cox J, Mann M. MaxQuant enables high peptide identification rates, individualized p.p.b.-range mass accuracies and proteome-wide protein quantification. Nat Biotechnol 2008;26:1367–72.

Godbout C, Follonier Castella L, Smith EA, Talele N, Chow ML, Garonna A, et al. The mechanical environment modulates intracellular calcium oscillation activities of myofibroblasts. PLoS One 2013;8:e64560.

Tyanova S, Temu T, Sinitcyn P, Carlson A, Hein MY, Geiger T, et al. The Perseus computational platform for comprehensive analysis of (prote)omics data. Nat Methods 2016;13:731–40.

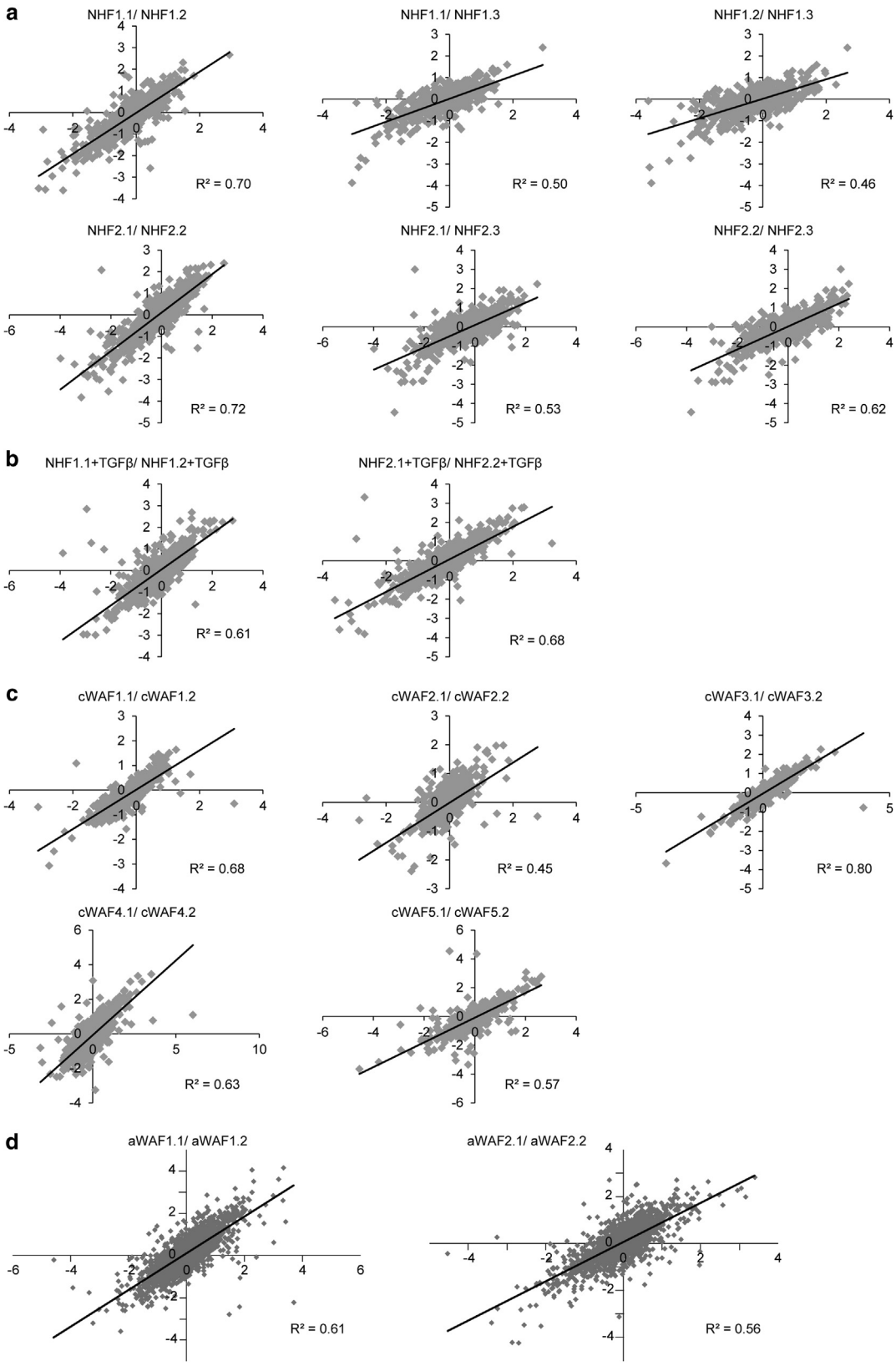

Supplementary Figure S1. Correlation of protein abundances between biological replicates. Shown are dot plots of $\log_2$-transformed SILAC ratios of label-swap experiments of biological replicates of (**a**) NHFs, (**b**) NHFs treated with TGFβ, (**c**) cWAFs, and (**d**) aWAFs compared with a SUPER-SILAC mix spike in. aWAF, acute wound–associated fibroblast; cWAF, chronic wound–associated fibroblast; NHF, normal human fibroblast; SILAC, stable isotope labeling by amino acids in cell culture.

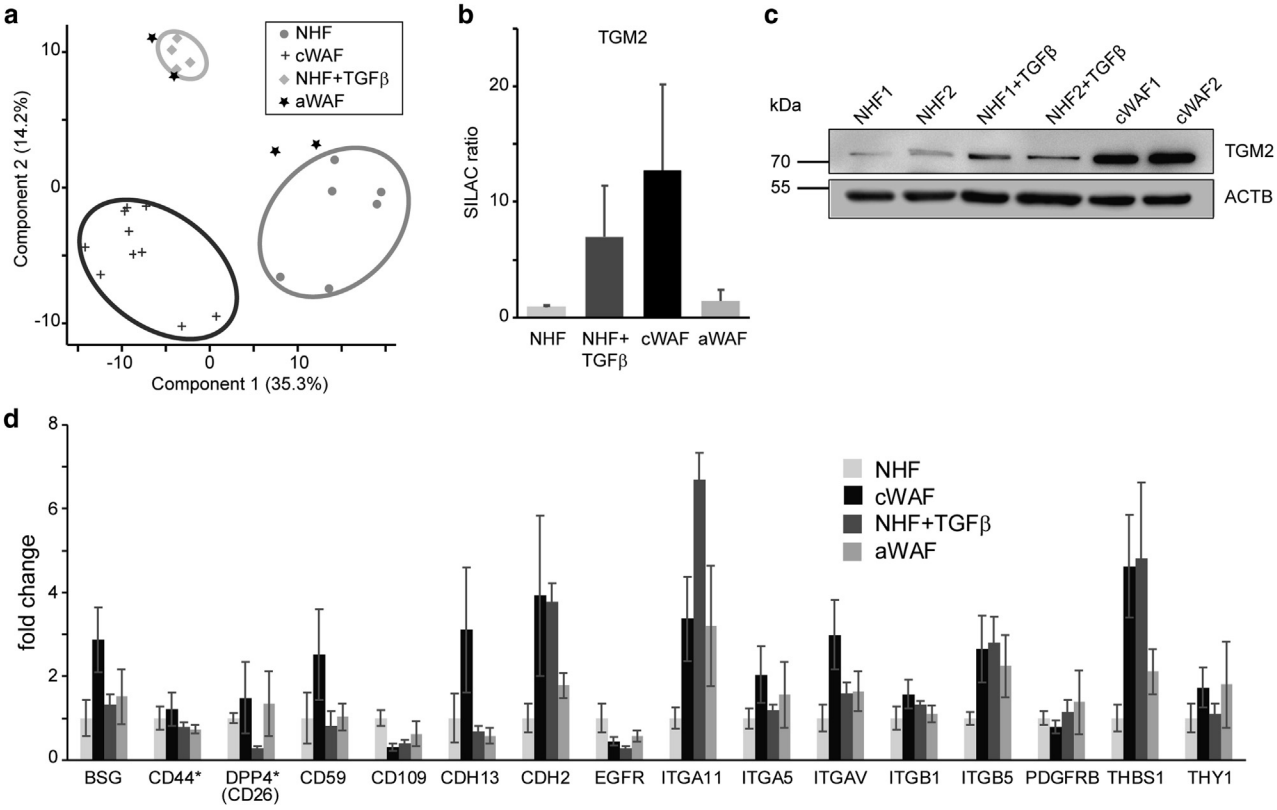

e

Gene Symbol	cWAF	NHF + TGFβ	aWAF
BSG	++	nc	nc
CD44*	nc	nc	nc
DPP4*	nc	- -	nc
CD59	++	nc	nc
CD109	- -	- -	-
CDH13	++	nc	nc
CDH2	++	++	+
EGFR	- -	- -	-
ITGA11	++	++	+
ITGA5	++	nc	nc
ITGAV	++	+	+
ITGB1	+	nc	nc
ITGB5	++	++	++
PDGFRB	-	nc	nc
THBS1	++	++	++
THY1	+	nc	nc

Supplementary Figure S2. cWAFs are a molecularly distinct fibroblast subtype. (**a**) PCA. Log_2-transformed SILAC ratios of proteins were used. Three experimental groups (cWAFs, NHFs, and NHFs + TGFβ) are clearly separated. aWAFs appear more heterogeneous, resembling NHFs or NHFs treated with TGFβ. (**b, c**) Bar diagram and western blot for TGM2. Protein abundances of TGM2 found by (b) LC-MS and (c) western blot are increased in cWAFs compared with aWAFs, TGFβ-treated, and control NHFs (Relative FC is normalized to the values of NHFs for (b); two-tailed, unpaired *t*-test, $^{**}P < 0.01$). (**d, e**) Surface protein abundance differences comparing NHFs, cWAFs, NHFs treated with TGFβ, and aWAFs. Cell surface markers that distinguish cWAFs, aWAFs, and TGFβ-treated cells from NHFs are displayed ($P < 0.05$, BH corrected, NHF vs. annotated cell type). nc: not changed compared with NHF; +, −: less than two-fold significantly changed compared with NHF; + +, − −: greater than two-fold significantly changed compared with NHF. Single asterisk indicates proteins that were defined as fibroblast lineage markers (Driskell et al., 2013). aWAF, acute wound–associated fibroblast; BH, Benjamini-Hochberg; cWAF, chronic wound–associated fibroblast; FC, fold change; LC, liquid chromatography; NHF, normal human fibroblast; PCA, principal component analysis; SILAC, stable isotope labeling by amino acids in cell culture.